

Semiconductor-metal transition in semiconducting bilayer sheets of transition-metal dichalcogenides

Swastibrata Bhattacharyya and Abhishek K. Singh*

Materials Research Centre, Indian Institute of Science, Bangalore 560012, India

(Received 29 March 2012; revised manuscript received 6 July 2012; published 24 August 2012)

Using first-principles calculations we show that the band gap of bilayer sheets of semiconducting transition-metal dichalcogenides (TMDs) can be reduced smoothly by applying vertical compressive pressure. These materials undergo a universal reversible semiconductor-to-metal (S-M) transition at a critical pressure. The S-M transition is attributed to lifting of the degeneracy of the bands at the Fermi level caused by interlayer interactions via charge transfer from the metal to the chalcogen. The S-M transition can be reproduced even after incorporating the band gap corrections using hybrid functionals and the GW method. The ability to tune the band gap of TMDs in a controlled fashion over a wide range of energy opens up the possibility for its usage in a range of applications.

DOI: [10.1103/PhysRevB.86.075454](https://doi.org/10.1103/PhysRevB.86.075454)

PACS number(s): 73.20.At, 73.40.Vz, 73.61.Le, 74.20.Pq

I. INTRODUCTION

Despite being a very promising two-dimensional (2D) material, gapless graphene has limitations for its applications in nanoelectronics and nanophotonics. This led to the finding of other 2D materials with finite band gap such as BN, transition-metal dichalcogenides (TMDs), and transition-metal oxides (MO_2). A BN sheet is an insulator, and modifying its band gap for optical and electronic applications is still a challenge. Depending on the combination of metal and chalcogen, TMDs offer a wide range of 2D materials: metals,^{1,2} superconductors,^{3,4} charge-density-wave systems,^{5,6} Mott insulators,⁷ and semiconductors.^{8,9} Semiconducting two-dimensional TMDs include MoS_2 , $MoSe_2$, $MoTe_2$, WS_2 , and WSe_2 and have emerged as promising materials for a range of applications.

Few layers to monolayers of MoS_2 and other TMDs have been successfully synthesized^{10–19} and their optical absorption and photoconductivity have been studied.^{10,20} A single layer of a TMD having stoichiometry of MX_2 consists of a hexagonally arranged transition metal ($M = Ti, Nb, Ta, Mo,$ or W) sandwiched between two layers of chalcogen atoms ($X = S, Se,$ or Te). Within a layer the metals and chalcogens form strong ionic-covalent bonds, whereas in bulk TMDs, the layers are bonded by weaker van der Waals (vdW) interaction. The bulk TMDs are indirect-band-gap semiconductors having band gaps in the range of 1.0–1.35 eV.⁸ With reduction in the number of layers the band gap increases⁹ and transforms into a direct gap for a single-layer TMD.^{21–23} In order to use these materials as building blocks in nanoelectronics, their electronic properties need to be modified. This has been achieved by doping^{1,24} and intercalation.^{25,26} TMD-based field-effect transistors with high room-temperature current on-off ratios²⁷ and higher on-current density^{28,29} as well as integrated circuits³⁰ have been successfully fabricated.

Tuning the band gaps of 2D materials—for their potential application in electromechanical devices, tunable photodetectors, and lasers—has been a challenge in band gap engineering. An applied strain or electric field offers a novel way of modifying the band gaps over a wide range. Even for graphene, it has been shown using density functional theory calculations that uniaxial strain on monolayers³¹ and applied vertical electric field to bilayers^{32–36} open a small band gap. Similar, theoretical studies for TMDs show a semiconductor-to-metal (S-M) transition for bilayers subjected to a vertical electric

field³⁷ (0.2–0.3 V/Å) and for mono- and bilayers under biaxial strain.³⁸ These techniques are promising but suffer from lack of practical applicability. For example, the electric field required to achieve the S-M transition is too large, and a reversible way of applying a biaxial strain in 2D materials has yet to be demonstrated in laboratory. On the other hand it has been experimentally shown that the band structure of bulk TMDs can be modified by application of compressive strain.³⁹ Here, we investigate the effect of normal compressive strain (NCS) on the electronic properties of semiconducting bilayer TMDs: MoS_2 , $MoSe_2$, $MoTe_2$, WS_2 , and WSe_2 . The band gaps of these materials decrease gradually with applied NCS. A reversible semiconductor-to-metal transition was observed after a threshold pressure P_{th} was achieved. The P_{th} depends upon the material as well as the stacking pattern of the two layers. The hybrid functional and GW methods were used to correct the Perdew-Burke-Ernzerhof (PBE) gap. The S-M transition was found to be independent of the method. This offers a wide range (1.9–0.0 eV) of reversible band gap tuning, which can be utilized for various applications.

II. COMPUTATIONAL DETAILS

The calculations were performed using *ab initio* density functional theory (DFT) in conjunction with all-electron projector augmented wave potentials^{40,41} and the Perdew-Burke-Ernzerhof⁴² generalized gradient approximation (GGA) to the electronic exchange and correlation, as implemented in the Vienna *ab initio* simulation package (VASP).⁴³ We optimize the structure of bilayer TMDs (MX_2 with $M = Mo, W$ and $X = S, Se, Te$), using the unit cells as shown in Fig. 1. A well-converged Monkhorst-Pack k -point set ($15 \times 15 \times 1$) was used for the calculation and the conjugate gradient scheme was employed to optimize the geometries until the forces on every atom were ≤ 0.005 eV/Å. Sufficient vacuum was used along the z direction, i.e., perpendicular to the 2D sheet, to avoid spurious interaction among the periodic images. The lattice parameters and interlayer distances of the optimized structures are listed in Table I and are in good agreement with the previously reported PBE values.¹

The weak van der Waals interaction between the layers has an effect in determining the interlayer distance for the bilayers as well as for the bulk MX_2 . The van der Waals

TABLE I. Structural parameters and band gaps of bulk, monolayer, and bilayer TMDs calculated using PBE and PBE + vdW functionals. For comparison purposes the corresponding experimental values are also included.

Material	Functional	Structural parameters (Å)				Band gap (eV)			
		a	c	Bilayer separation		Bulk	Monolayer	Bilayer	
				AB	AA				AB
MoS ₂	PBE	3.18	12.42 ^a	4.14	4.54	0.94	1.68	1.59	1.63
	PBE + vdW	3.21	12.42	3.11	3.72	0.85 1.25	1.47		
	Expt.	3.16 (Ref. 44)	12.29 (Ref. 44)			1.23 (Ref. 8)	1.9 (Ref. 45)	1.6 (Ref. 45)	
MoSe ₂	PBE	3.32	13.06 ^a	3.88	4.36	0.87	1.43	1.42	1.41
	PBE + vdW	3.33	13.06	3.19	3.78	0.87		1.18	1.41
	Expt.	3.30 (Ref. 44)	12.94 (Ref. 44)			1.09 (Ref. 8)			
MoTe ₂	PBE	3.56	13.95 ^a	3.95	4.97	0.67	1.06	1.03	1.05
	PBE + vdW	3.54	13.95	3.37	4.07	0.68		0.88	1.02
	Expt.	3.52 (Ref. 44)	13.97 (Ref. 44)			1.00 (Ref. 44)			
WS ₂	PBE	3.18	12.99 ^a	4.31	4.56	1.25	1.81	1.77	1.79
	PBE + vdW	3.19	12.99	3.39	3.95	1.24		1.57	1.70
	Expt.	3.15 (Ref. 46)	12.32 (Ref. 46)			1.35 (Ref. 8)			
WSe ₂	PBE	3.32	13.38 ^a	4.11	4.43	1.09	1.53	1.51	1.52
	PBE + vdW	3.34	13.38	3.35	3.98	1.08		1.43	1.51
	Expt.	3.28 (Ref. 46)	12.96 (Ref. 46)	-	-	1.20 (Ref. 8)			

^aSame values as for vdW calculation.

interaction originates from dynamical correlations between fluctuating charge distributions and cannot be described by the PBE functional. Consequently, the relaxed bilayer distance obtained by PBE is off by approximately 1 Å compared to the bulk interlayer distance. We incorporate the van der Waals interactions by adding a semi-empirical dispersion potential (D) to the conventional Kohn-Sham DFT energy, through a pair-wise force field following Grimme's DFT-D2 method⁴⁷ (where D2 stands for the second generation of this method). The parameters used in the DFT-D2 method are thoroughly optimized for several of the DFT functionals, including the PBE functional. We performed a comprehensive test of the reliability of the empirical parameters by calculating the bulk phase of the TMDs. The lattice parameters obtained using this approach are in very good agreement with the experimental values;^{44,46} see Table I. The calculated DFT-D2 interlayer

distances in bilayer TMDs have decreased significantly compared with the PBE results (Table I).

III. RESULTS AND DISCUSSION

The two layers in a bilayer TMD can be arranged in either AA or AB stacking. In the AA (AB) stacking the M atoms in one layer are on top of the M (X) atoms in another layer (Fig. 1). AB stacking is preferred in both bulk and bilayer TMDs. In the case of a bilayer TMD the energy differences between the two types of stacking are very small. Therefore, in the current work, the effect of applied normal compressive strain on the band structure of both AA - and AB -stacked TMDs was studied. The strain was calculated as $\varepsilon = (d_0 - d)/d_0$, where d_0 and d are the equilibrium and instantaneous interlayer distances, respectively. A constrained relaxation scheme, where the positions of the metal atoms remained unchanged, was used for the optimization of the structures. This prevented the relaxation of instantaneous structures to the original positions. All the reported results here onwards include the vdW interactions via the DFT-D2 method, unless otherwise mentioned.

The overall behavior of the band structure under the applied pressure remains similar for both type of stacking. Therefore, here we will present mainly the results of AB -stacked TMDs. The PBE + vdW band structure calculations show that the unstrained bilayers of all these AB -stacked TMDs are indirect-band-gap semiconductors. In comparison to a monolayer, the band gap of a bilayer decreases slightly and each band becomes doubly degenerate as shown in Fig. 2 for MoS₂. This clearly demonstrates the absence of chemical interaction between the

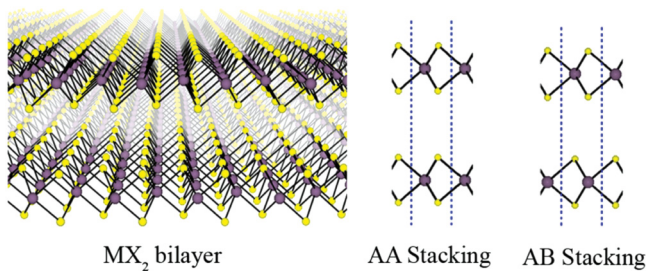


FIG. 1. (Color online) Structure of AB -stacked MX_2 bilayer with M and X atoms are shown by purple (larger) and yellow (smaller) spheres, respectively. Side view of the bilayers with AA and AB stacking. The blue dotted lines show the unit cells.

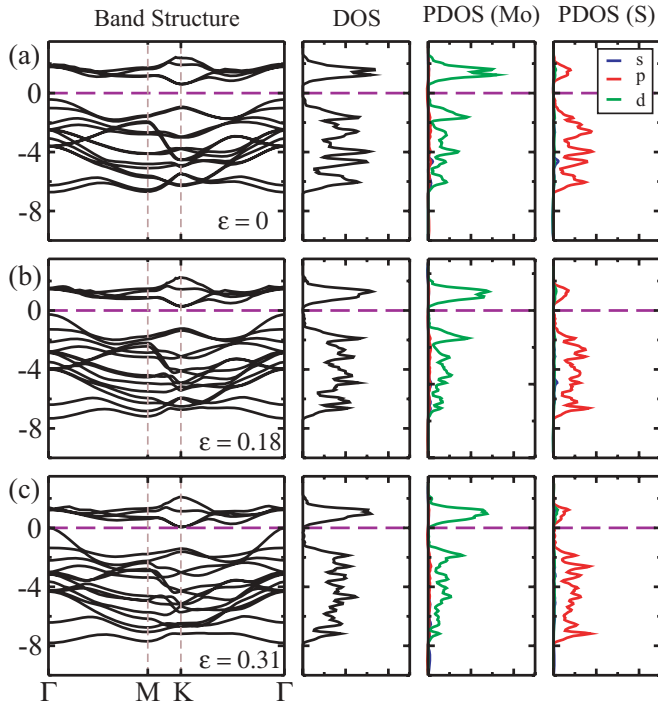


FIG. 2. (Color online) Band structure, total density of states (DOS), and projected densities of states (PDOSs) of Mo and S for MoS₂ bilayer at (a) 0, (b) 0.18, and (c) 0.31 strain.

layers. As the interlayer separation decreases, the layers start to interact chemically, which leads to lifting of the double degeneracy of the bands (Fig. 2). This splitting increases with increasing NCS. The valence band maximum (VBM) moves away (towards) the Fermi level at the *K* (Γ) point. The S-M transition occurs when the VBM crosses the Fermi level at the Γ point after a critical applied NCS. Likewise, the conduction band minimum (CBM) also moves towards the Fermi level with increasing NCS. The band structures of the other MX_2 materials undergo similar changes (lifting of double degeneracy and a S-M transition) under applied NCS. The interlayer distance at which the S-M transition takes place is listed in Table II for the bilayers.

In order to determine the constituents of the electronic bands, the total and projected density of states (PDOSs) were calculated for the bilayers under various NCS values and are shown for MoS₂ in Fig. 2. The total DOS shows a gap near

the Fermi level, which is reduced due to the shift of the CBM and the VBM towards the Fermi level with increase in strain. For the unstrained MoS₂, the CBM and the VBM are constituted by Mo *d* and S *p* orbitals, which can be clearly seen from the PDOSs. With increasing NCS, the contributions to the CBM from Mo *d* and S *p* orbitals decrease, while that from S *d* increases. The change in the band gap as a function of applied NCS follows a similar pattern for all the materials studied here [Fig. 3(a)]. This change is reversible, i.e., in the absence of applied pressure the structure relaxes back to the original structure with complete recovery of the band gap, which is very important for sensor applications. Similar changes in band gap⁴⁸ and resistance³⁹ were reported for bulk MoS₂ under applied pressure, but unlike for bilayers no S-M transition was observed even at very high pressure (40 GPa).

In order to access the feasibility of S-M transition in experiments, the applied pressure (P) was calculated from the energy cost per unit area in reducing the interlayer distance by $\Delta d = (d_0 - d)$ as per the following equation:

$$P = \frac{E - E_0}{(d_0 - d)A}, \quad (1)$$

where A is the area of the unit cell, and E and E_0 are the energies and d and d_0 the interlayer distances of the strained and unstrained bilayers. The pressure required for the S-M transition, P_{th} , for each material is listed in Table II. The calculated pressure range is easily achievable experimentally, and hence makes tuning of the band gap via NCS very attractive for various applications. The percentage reduction in band gap with increase in pressure is plotted in Fig. 4. The plot is linear for most of the bilayers except for *AB*-stacked WX_2 . For MoTe₂, the change in band gap is much less initially but increases greatly after a pressure of 1.3 GPa. The slope and hence the response of the change in band gap to applied pressure for MoTe₂ (*AB*) is the largest among all the TMDs. Surprisingly, the S-M transition occurs at relatively lower pressure for the *AA* stacking than the *AB* except for MoTe₂. For a given metal atom, the S-M transition pressure decreases as we go down the column of *X* atoms in the periodic table. This is caused by increased delocalization of the atomic orbitals, which leads to reduced interaction between *M* and *X* atoms, resulting in a S-M transition at lower pressure. Such behavior is consistent with the trend of the band gap, which also decreases from S to Te (Table I).

TABLE II. Interlayer distance and pressure required for semiconductor-to-metal transition, P_{th} , of TMDs for both *AA* and *AB* stacking calculated using the vdW forces.

Material	Bilayer separation at transition (\AA)		Transition pressure (P_{th}) (GPa)	
	<i>AB</i>	<i>AA</i>	<i>AB</i>	<i>AA</i>
MoS ₂	2.14	2.60	8.52, 14.47 ^a	8.37
MoSe ₂	2.23	2.64	8.37	9.54
MoTe ₂	2.69	2.93	5.10	8.71
WS ₂	1.80	2.47	16.28	10.54
WSe ₂	2.21	2.79	15.83	12.28

^aHSE value.

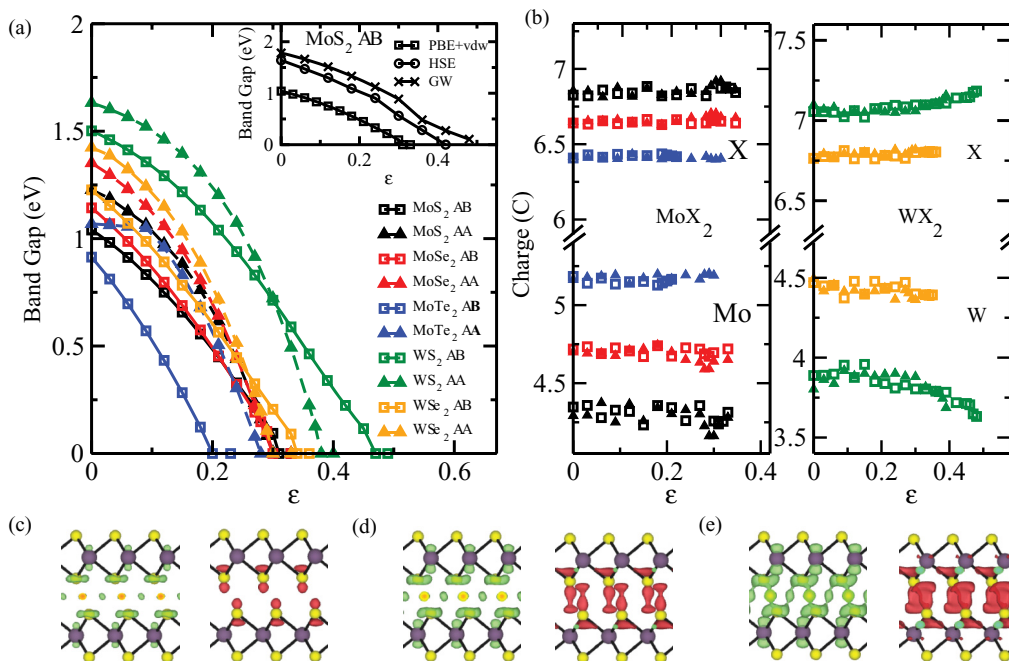


FIG. 3. (Color online) (a) Change in band gap with applied strain for MX_2 bilayers for both AA and AB stacking using the PBE + vdW method. The inset shows the same using the PBE + vdW, HSE, and GW methods for an AB-stacked MoS₂ bilayer. (b) Average Bader charge of M and X for all the bilayers as a function of strain. The left and right panels correspond to $M = \text{Mo}$ and W , respectively. The same color and symbols are used for the respective bilayers as defined in (a). Isosurfaces of charge accumulation (green) and depletion (red) of MoS₂ bilayer under strain of (c) 0.18, (d) 0.24, and (e) 0.31.

Similar evidence also comes from a Bader charge analysis.^{49–51} The average charge on M and X as a function of applied strain is shown in Fig. 3(b). The charge transfer from M to X increases as a function of NCS, a change which is more prominent for WX_2 . Furthermore, for a given M atom, the value of the average charge on the X atom decreases as we go down the periodic table, i.e., from S to Te, replicating

closely the trend of electron affinity of the X atoms. This, essentially, results in a weaker interaction between the M and X atoms, which leads the S-M transition pressure to be lowest for Te and highest for S. Furthermore, in comparison to W, Mo has a lower ionization potential, which measures the ability to donate charge. Mo can donate charges relatively easily and thereby facilitate the X - X interaction, which results in a S-M transition in MoX₂ at lower pressure than in WX₂.

These conclusions were further supported by the redistribution of charges, which was calculated by taking the difference of the total charge of the bilayer and two isolated layers for MoS₂, as shown in Figs. 3(c)–3(e). The maximum redistribution of the charge occurs around the inner S atoms and the adjacent Mo-S bonds. As expected, for low strains (below $\epsilon = 0.21$) no charge rearrangement was observed. At the nonzero strains, the charge started accumulating on the inner S atoms as well as on adjacent Mo-S bonds [Figs. 3(c)–3(e)]. However, the charge depletion was observed predominantly from the inner S atoms. With increasing NCS, the amount of charge redistribution also increases, indicating an enhanced S-S interaction, which essentially causes the S-M transition. Due to the smaller S-S distances the interaction is better for the AA stacking than for the AB. This is why P_{th} for AA stacking is lower than for AB stacking.

In order to gain further insight, the band-decomposed electron densities of the VBM and CBM at different strains are plotted and shown in Fig. 5. Consistent with the above analysis, the VBM originates from the interaction of inner S atoms and adjacent Mo-S bonds [Fig. 5(a)]. With the increasing interaction caused by the applied NCS, the contribution from the inner S atoms further increases. The VBM is extended and

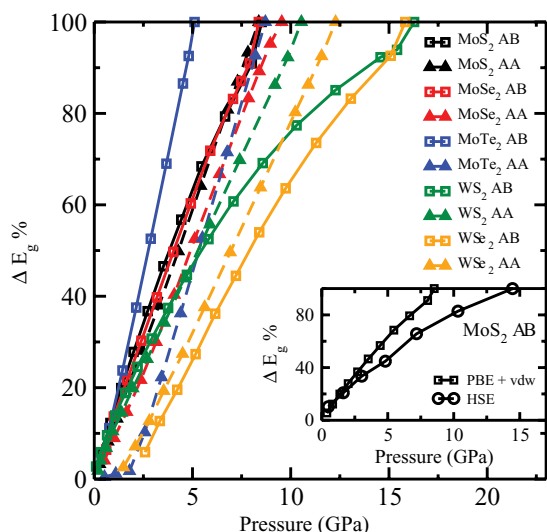


FIG. 4. (Color online) Percentage change in band gap with applied pressure for MX_2 bilayers obtained using the PBE + vdW method. Inset: The same plot using PBE + vdW and HSE methods for an AB-stacked MoS₂ bilayer.

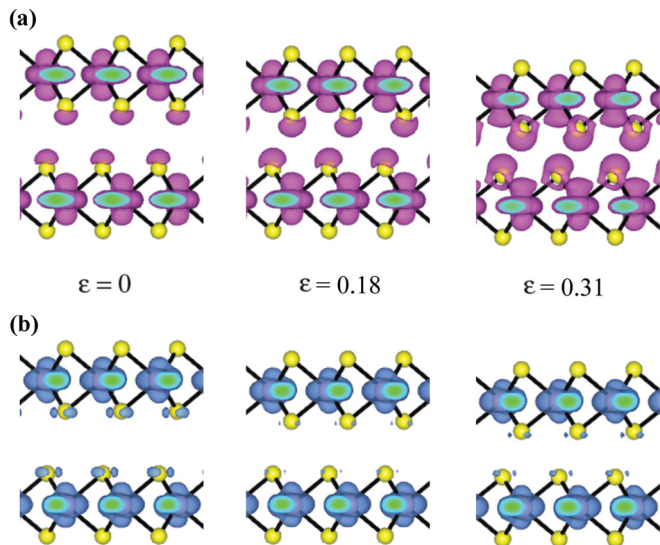


FIG. 5. (Color online) Isosurfaces of band-decomposed charge density of (a) valence band maximum and (b) conduction band minimum of an AB -stacked MoS_2 bilayer at applied strain of 0, 0.18, and 0.31, respectively.

hence the effective mass does not change much even after the application of NCS, implying maintenance of the quality of the conductivity. Furthermore, the lowering of the symmetry of the VBM is also evident. The CBM completely originates from the Mo-S bonds [Fig. 5(b)]. Once again the nature is more extended and hence will keep the conductivities intact. The modification of the gap without significant alteration of the dispersion of the bands is very important for electronic applications.

Due to the presence of artificial self-interaction⁵² and the absence of derivative discontinuity in the exchange-correlation potential, DFT in the local-density approximation (LDA) and GGA suffers from underestimation of the band gap. The calculated PBE-GGA band gap of bulk, monolayer, and bilayer MoS_2 is underestimated by an amount of 0.29 eV (23.7%), 0.22 eV (11.5%), and 0.01 eV (0.5%), respectively, compared to the experimental values (Table I). The excellent agreement for the bilayer is misleading as it corresponds to a wrong geometry (extremely large c value) obtained with the PBE functional in the absence of vdW interactions. The band gap of a bilayer with the geometry optimized by the PBE + vdW functional is underestimated by 0.33 eV (20.6%) with respect to the experimental value. For comparison, the band gap using the LDA functional was also calculated for MoS_2 . The LDA predicts the correct band gap for the monolayer but gives values 0.47 eV (38.4%) and 0.66 eV (41.1%) lower than the experimental ones for the bulk and bilayer MoS_2 respectively.

In order to correct the PBE band gaps, we used a hybrid Heyd-Scuseria-Ernzerhof^{53,54} (HSE) functional. In the HSE approach, the exchange potential is separated into a long-range and a short-range part. 1/4 of the PBE exchange is replaced by the Hartree-Fock exact exchange and the full PBE correlation energy is added. The HSE functional is shown to correct the GGA band gaps^{53,55} significantly by partially correcting the self-interaction. However, the results are system dependent. The calculated band gap for a MoS_2 bilayer using the HSE

functional is 1.64 eV, which is in very good agreement with the experimental value (1.60 eV).

We also corrected the PBE band gaps by using DFT with many-body perturbation theory in the GW approximation.⁵⁶ A partially self-consistent GW0 method was used in which the G was iterated but the W was kept fixed to the initial DFT (PBE) W_0 . A default cutoff (280.0 eV) for the wave function was used for the GW calculation. A convergence study was performed for the number of bands, k points, and frequency grid points to achieve a convergence within 10–20 meV for the band gaps. A Γ -centered Monkhorst-Pack k -point grid of $18 \times 18 \times 1$ mesh was used for calculating the GW band structure. Like the HSE functional, the GW0 also improves the PBE band gap overestimating it by 0.18 eV (11.3%) (for the bilayer) compared with the experimental value. The GW0 band gap is slightly larger than the HSE gap. There are not many experimental results for the band gaps of the 2D materials. Furthermore, the quality of as-grown 2D sheets can also play an important role in band gap determination. In order to get a more reliable comparison more experiments are required. The band gap calculated using the HSE functional is the closest to the experimental value among all the methods used in this work for bilayer MoS_2 . Both HSE and GW calculations are computationally very expensive and hence we applied these methods only to MoS_2 .

We checked the robustness of the S-M transition by calculating the band structure of MoS_2 as a function of normal compressive strain using the HSE functional and the GW method. A plot of the HSE and GW band gaps as a function of applied strain is compared with the one for the PBE + vdW in Fig. 3(a) inset. A comparison of the percentage reduction in band gap with increase in pressure for different materials and methods is shown in Fig. 4. Although the calculated HSE and GW band gaps of MoS_2 were slightly larger than the PBE gap, the nature of the band structure as well as the S-M transition remained unchanged. Since the band gap obtained from HSE and GW calculations was slightly greater than those with the GGA, an increase in transition interlayer distance (as well as P_{th} for the HSE functional) was observed for the S-M transition. The excellent agreement between the HSE and experimental band gaps suggests that the transition temperature would be closer to the HSE values. However, more experiments are required to claim good numerical accuracy.

IV. CONCLUSION

In conclusion, we report reversible band gap engineering of semiconducting bilayers of transition-metal dichalcogenides by applied normal compressive strain. The band gap can be tuned in a large energy range without modifying the conductivity significantly. Furthermore, a universal reversible semiconductor-to-metal transition was observed for all the semiconducting TMDs. The reduction of the gap as a function of applied pressure is caused by interlayer interaction, which eventually lifts the degeneracies of the bands and moves them closer to the Fermi level. For a given M in MX_2 , the threshold pressure P_{th} needed to achieve the S-M transition decreases as X changes from S to Te. Furthermore, MoX_2 has lower P_{th} compared with WX_2 . The PBE band gap of MoS_2 was corrected using the hybrid HSE functional and the GW method.

The S-M transition can be reproduced even after applying the band gap corrections, but the P_{th} changes to a larger value. The tantalizing possibility of reversible tuning by more than 1.9 eV of the energy gap by applying compressive strain, as shown in the present work, would make the TMDs useful in a wide range of applications spanning from sensors to electronics.

ACKNOWLEDGMENTS

AKS thankfully acknowledge financial support from the Board of Research in Nuclear Sciences Grant No. 2011/37C/51/BRNS, and National Program on Micro and Smart Systems (NpMASS) PARC No. 1:22.

*abhishek@mrc.iisc.ernet.in

- ¹Y. Ding, Y. Wang, J. Ni, L. Shi, S. Shi, and W. Tang, *Physica B* **406**, 2254 (2011).
- ²A. Ayari, E. Cobas, O. Ogundadegbe, and M. S. Fuhrer, *J. Appl. Phys.* **101**, 014507 (2007).
- ³A. M. Gabovich, A. I. Voitenko, J. F. Annett, and M. Ausloos, *Supercond. Sci. Technol.* **14**, R1 (2001).
- ⁴E. Morosan, H. W. Zandbergen, B. S. Dennis, J. W. G. Bos, Y. Onose, T. Klimczuk, A. P. Ramirez, N. P. Ong, and R. J. Cava, *Nat. Phys.* **2**, 544 (2006).
- ⁵K. Rossnagel, O. Seifarth, L. Kipp, M. Skibowski, D. Voß, P. Krüger, A. Mazur, and J. Pollmann, *Phys. Rev. B* **64**, 235119 (2001).
- ⁶W. Z. Hu, G. Li, J. Yan, H. H. Wen, G. Wu, X. H. Chen, and N. L. Wang, *Phys. Rev. B* **76**, 045103 (2007).
- ⁷A. F. Kusmartseva, A. Akrap, H. Berger, L. Forro, and E. Tutis, *Nat. Mater.* **7**, 960 (2008).
- ⁸K. K. Kam and B. A. Parkinson, *J. Phys. Chem.* **86**, 463 (1982).
- ⁹S. W. Han, H. Kwon, S. K. Kim, S. Ryu, W. S. Yun, D. H. Kim, J. H. Hwang, J.-S. Kang, J. Baik, H. J. Shin, and S. C. Hong, *Phys. Rev. B* **84**, 045409 (2011).
- ¹⁰R. F. Frindt and A. D. Yoffe, *Proc. R. Soc. London, Ser. A* **273**, 69 (1963).
- ¹¹K. S. Novoselov, D. Jiang, F. Schedin, T. J. Booth, V. V. Khotkevich, S. V. Morozov, and A. K. Geim, *Proc. Natl. Acad. Sci. USA* **102**, 10451 (2005).
- ¹²R. F. Frindt, *J. Appl. Phys.* **37**, 1928 (1966).
- ¹³P. Joensen, R. F. Frindt, and S. R. Morrison, *Mater. Res. Bull.* **21**, 457 (1986).
- ¹⁴A. Schumacher, L. Scandella, N. Kruse, and R. Prins, *Surf. Sci.* **289**, L595 (1993).
- ¹⁵J. N. Coleman *et al.*, *Science* **331**, 568 (2011).
- ¹⁶B. K. Miremadi and S. R. Morrison, *J. Appl. Phys.* **63**, 4970 (1988).
- ¹⁷D. Yang and R. Frindt, *J. Phys. Chem. Solids* **57**, 1113 (1996).
- ¹⁸H. S. S. Ramakrishna Matte, A. Gomathi, A. K. Manna, D. J. Late, R. Datta, S. K. Pati, and C. N. R. Rao, *Angew. Chem. Int. Ed.* **49**, 4059 (2010).
- ¹⁹G. Eda, H. Yamaguchi, D. Voiry, T. Fujita, M. Chen, and M. Chhowalla, *Nano Lett.* **11**, 5111 (2011).
- ²⁰T. Korn, S. Heydrich, M. Hirmer, J. Schmutzler, and C. Schuller, *Appl. Phys. Lett.* **99**, 102109 (2011).
- ²¹S. Lebégue and O. Eriksson, *Phys. Rev. B* **79**, 115409 (2009).
- ²²A. Splendiani, L. Sun, Y. Zhang, T. Li, J. Kim, C.-Y. Chim, G. Galli, and F. Wang, *Nano Lett.* **10**, 1271 (2010).
- ²³J. K. Ellis, M. J. Lucero, and G. E. Scuseria, *Appl. Phys. Lett.* **99**, 261908 (2011).
- ²⁴D. S. Inosov, V. B. Zabolotnyy, D. V. Evtushinsky, A. A. Kordyuk, B. Büchner, R. Follath, H. Berger, and S. V. Borisenko, *New J. Phys.* **10**, 125027 (2008).
- ²⁵T. Kidd, D. Klein, T. Rash, and L. Strauss, *Appl. Surf. Sci.* **257**, 3812 (2011).
- ²⁶A. Colev, C. Gherman, V. Mirovitskii, L. Kulyuk, and E. Fortin, *J. Lumin.* **129**, 1945 (2009).
- ²⁷B. Radisavljevic, A. Radenovic, J. Brivio, V. Giacometti, and A. Kis, *Nat. Nanotechnol.* **6**, 147 (2010).
- ²⁸L. Liu, S. Kumar, Y. Ouyang, and J. Guo, *IEEE Trans. Electron Devices* **58**, 3042 (2011).
- ²⁹Y. Yoon, K. Ganapathi, and S. Salahuddin, *Nano Lett.* **11**, 3768 (2011).
- ³⁰B. Radisavljevic, M. B. Whitwick, and A. Kis, *ACS Nano* **5**, 9934 (2011).
- ³¹Z. H. Ni, T. Yu, Y. H. Lu, Y. Y. Wang, Y. P. Feng, and Z. X. Shen, *ACS Nano* **2**, 2301 (2008).
- ³²E. McCann, *Phys. Rev. B* **74**, 161403 (2006).
- ³³E. V. Castro, K. S. Novoselov, S. V. Morozov, N. M. R. Peres, J. M. B. Lopes dos Santos, J. Nilsson, F. Guinea, A. K. Geim, and A. H. Castro Neto, *Phys. Rev. Lett.* **99**, 216802 (2007).
- ³⁴T. Ohta, A. Bostwick, T. Seyller, K. Horn, and E. Rotenberg, *Science* **313**, 951 (2006).
- ³⁵Y. Zhang, T.-T. Tang, C. Girit, Z. Hao, M. C. Martin, A. Zettl, M. F. Crommie, Y. R. Shen, and F. Wang, *Nature (London)* **459**, 820 (2009).
- ³⁶F. Xia, D. B. Farmer, Y.-m. Lin, and P. Avouris, *Nano Lett.* **10**, 715 (2010).
- ³⁷A. Ramasubramaniam, D. Naveh, and E. Towe, *Phys. Rev. B* **84**, 205325 (2011).
- ³⁸E. Scalise, M. Houssa, G. Pourtois, V. Afanas'ev, and A. Stesmans, *Nano Res.* **5**, 43 (2012).
- ³⁹M. Dave, R. Vaidya, S. G. Patel, and A. R. Jani, *Bull. Mater. Sci.* **27**, 213 (2004).
- ⁴⁰P. E. Blöchl, *Phys. Rev. B* **50**, 17953 (1994).
- ⁴¹G. Kresse and D. Joubert, *Phys. Rev. B* **59**, 1758 (1999).
- ⁴²J. P. Perdew, K. Burke, and M. Ernzerhof, *Phys. Rev. Lett.* **77**, 3865 (1996).
- ⁴³G. Kresse and J. Hafner, *Phys. Rev. B* **47**, 558 (1993).
- ⁴⁴T. Böker, R. Severin, A. Müller, C. Janowitz, R. Manzke, D. Voß, P. Krüger, A. Mazur, and J. Pollmann, *Phys. Rev. B* **64**, 235305 (2001).
- ⁴⁵K. F. Mak, C. Lee, J. Hone, J. Shan, and T. F. Heinz, *Phys. Rev. Lett.* **105**, 136805 (2010).
- ⁴⁶W. Schutte, J. D. Boer, and F. Jellinek, *J. Solid State Chem.* **70**, 207 (1987).
- ⁴⁷S. Grimme, *J. Comput. Chem.* **27**, 1787 (2006).
- ⁴⁸L. Wei, C. Jun-fang, H. Qinyu, and W. Teng, *Physica B* **405**, 2498 (2010).

- ⁴⁹W. Tang, E. Sanville, and G. Henkelman, *J. Phys.: Condens. Matter* **21**, 084204 (2009).
- ⁵⁰E. Sanville, S. D. Kenny, R. Smith, and G. Henkelman, *J. Comput. Chem.* **28**, 899 (2007).
- ⁵¹G. Henkelman, A. Arnaldsson, and H. Jónsson, *Comput. Mater. Sci.* **36**, 354 (2006).
- ⁵²J. P. Perdew and A. Zunger, *Phys. Rev. B* **23**, 5048 (1981).
- ⁵³J. Heyd, G. E. Scuseria, and M. Ernzerhof, *J. Chem. Phys.* **118**, 8207 (2003).
- ⁵⁴J. Heyd, G. E. Scuseria, and M. Ernzerhof, *J. Chem. Phys.* **124**, 219906 (2006).
- ⁵⁵Y.-i. Matsushita, K. Nakamura, and A. Oshiyama, *Phys. Rev. B* **84**, 075205 (2011).
- ⁵⁶L. Hedin, *Phys. Rev.* **139**, A796 (1965).